

1 Comparison of a Semi-Implicit and a Fully-Implicit Time Integration Method for a
2 Highly Degenerate Diffusion-Reaction Equation Coupled with an Ordinary
3 Differential Equation

4 by

5 Eric M. Jalbert

6 A Thesis
7 presented to
8 The University of Guelph

9 In partial fulfilment of requirements
10 for the degree of
11 Master of Science
12 in
13 Applied Mathematics

14 Guelph, Ontario, Canada

15 © E.M. Jalbert, January, 2015

16 Contents

17 1 Simulation Results	1
18 1.1 Typical Simulation	1
19 1.2 Travelling Wave Analysis	7
20 1.3 Spatial Effects	17
21 Bibliography	22
22 A Default Parameter Values	24

²³ **Chapter 1**

²⁴ **Simulation Results**

²⁵ Now that the method has been sufficiently validated and tested it can be used to generate observations
²⁶ of certain characteristics in the model. A generic simulation is set up so that the typical behaviour of
²⁷ the system can be observed.

²⁸ **1.1 Typical Simulation**

²⁹ A typical simulation refers to the parameter values and the choice of initial condition. It will show the
³⁰ behaviour of the system under normal circumstances and help reveal the interesting characteristics.

³¹ The typical initial condition attempts to emulate the biological situation of biomass growing inwards
³² on a sheet of cellulose. This will show how the biomass moves and how two separate masses interact
³³ in a collision. The initial condition used will initialize a number of random spherical inoculation
³⁴ points near the $y = 0$ and $y = 1$ axis. We let (x_r, y_r) be the random point used as the center for
³⁵ inoculation. To separate the inoculation points we have $x_r \in [0, 1]$ and $y_r \in [0, 0.1] \cup [0.9, 1]$. The
³⁶ number of inoculation points are the same for both the $y = 0$ region and $y = 1$ region. Multiple
³⁷ inoculation points combine additively. Each spherical inoculation point is computed as,

³⁸
$$M = \frac{-h}{d^2} ((x - x_r)^2 + (y - y_r)^2) + h, \quad M \geq 0. \quad (1.1)$$

39 The choice of parameter value is based on the default values given in Table A.1. There are 40 innoc-
 40 ulation points of both sides, totalling 80. The fully-implicit method is used here with $tol = 10^{-8}$.

41 **1.1.1 Biomass Ratio**

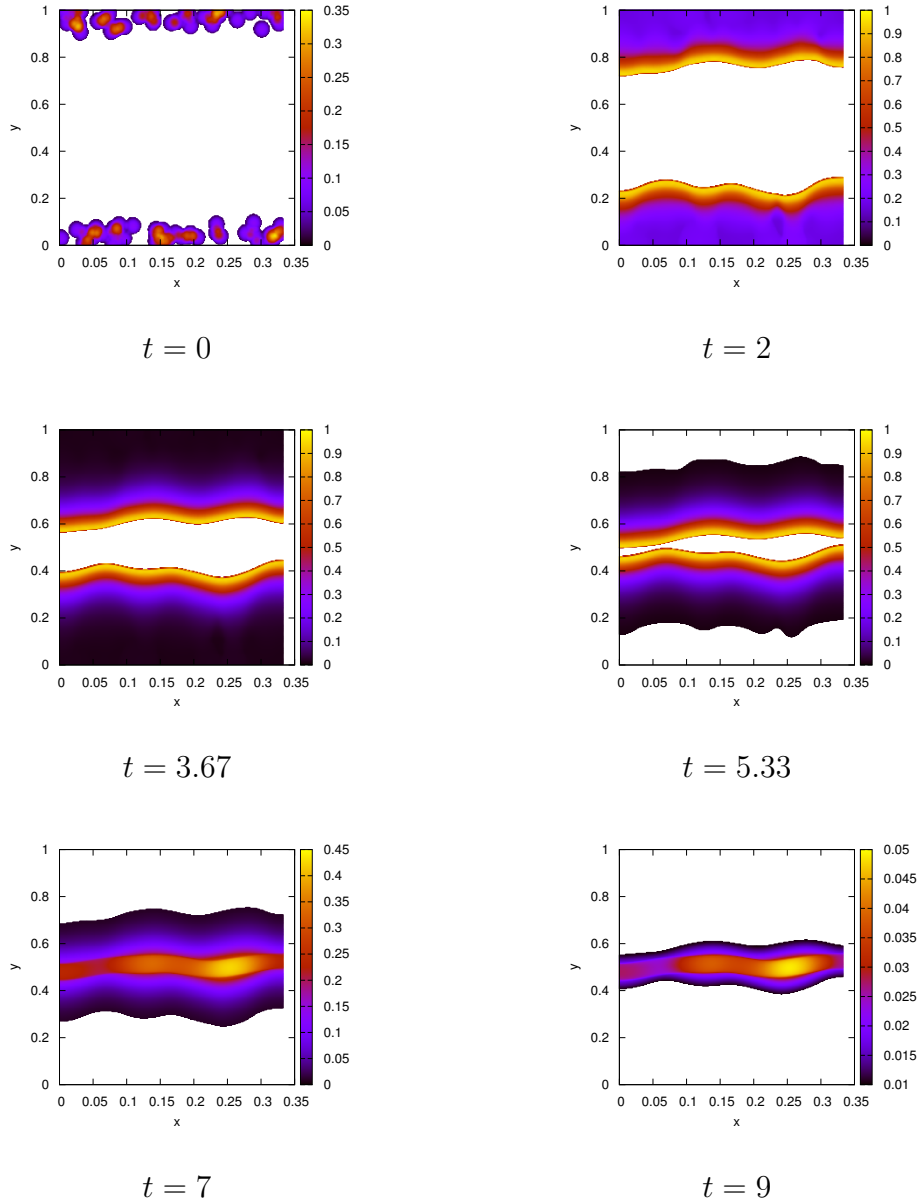


Figure 1.1: A graph showing the M solution of a typical simulation at different time steps. The initial condition is 80 random spherical innoculation points evenly divided between each of the $y = 0$ and $y = 1$ sides. A 513×513 grid was used.

42 Figure 1.1 shows the time evolution of M for the simulation. Here, the random innoculations on both

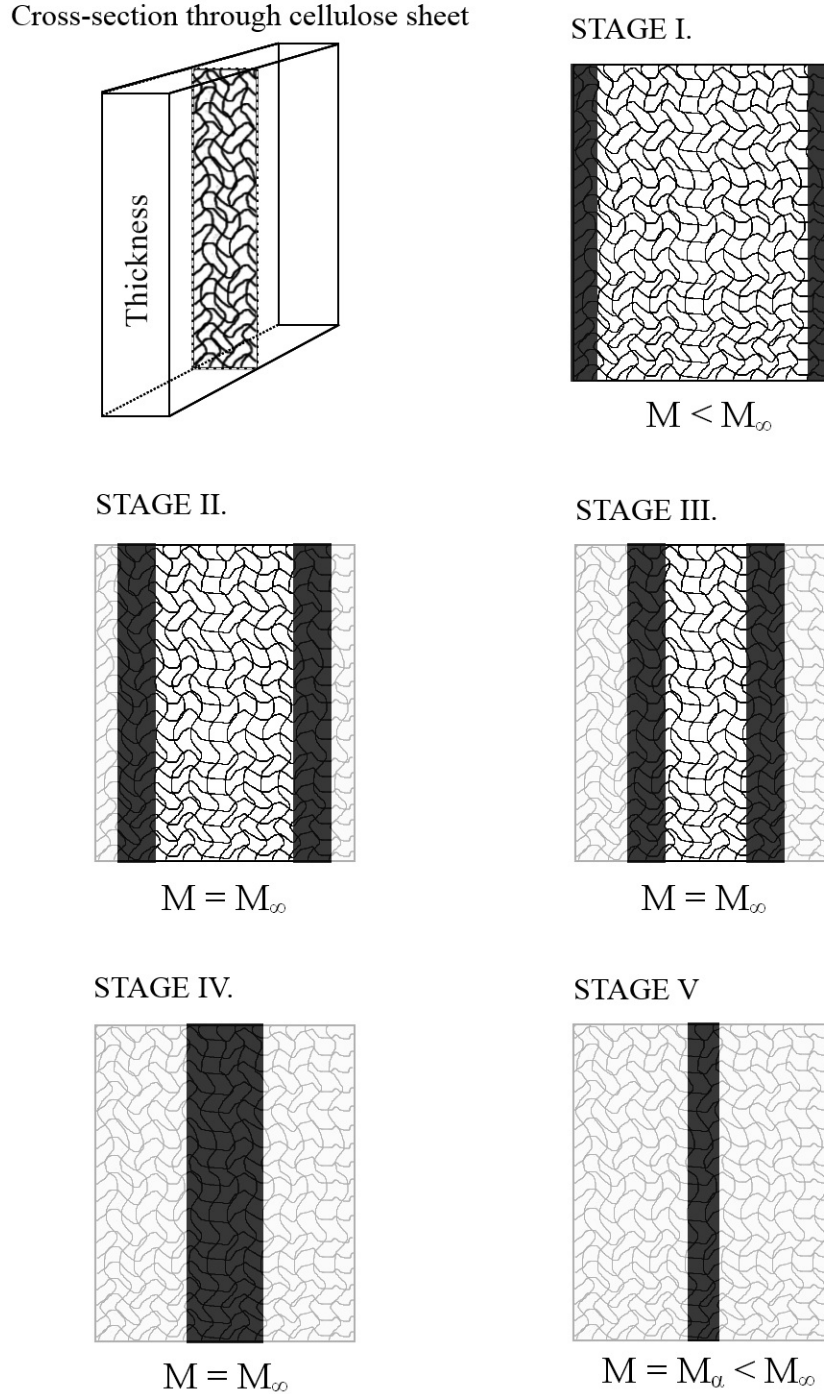


Figure 1.2: Conceptual model of cellulolytic biofilm growth and consumption of cellulose sheets. Attachment and growth occurs on both sides of the sheet, individual monolayers form on each fiber and result in a band of active biofilm (i.e., the effective sessile biomass) M (dark band). The ideal carrying capacity is M_∞ and the actual carrying capacity is M_a are explained in Dumitrache (2014). Consumed substrate is represented by the light gray areas.

⁴³ sides of region propagate towards each other and eventually combine at the center. By looking at

⁴⁴ $t = 2$, $t = 3.67$, and $t = 5.33$ it appears as though the wave front is moving with a constant shape and

- 45 at a constant speed. This suggest that there may be the existence of a travelling wave solution.
- 46 One important feature to notice is that the time evolution in Figure 1.1 matches the conceptual model
 47 proposed in Dumitrache (2014). This model can be seen in Figure 1.2. The different stages of the
 48 conceptual model can be observed in our simulation results:
- 49 • Stage I: $t = 2$ and $t = 3.67$ show the biomass growing towards the center of the sheet, which is
 50 the center white area.
- 51 • Stage II/III: $t = 5.33$ shows the consumed substate region as the outer white.
- 52 • Stage IV: Not shown. Only occurs at the moment when the two band first collide and the
 53 biomass concetration at that point still remains at the actual carrying capacity.
- 54 • Stage V: $t = 7$ and $t = 9$ show the combined center band, now at a biomass concentration
 55 lower then the actual carrying capacity.

56 Some important quantities to track are the total amount of biomass, M , and substrate, C . These values
 57 will be called $T_M(t)$ and $T_C(t)$ to represent the total biomass and total substrate, respectively. The
 58 computation for these values can be done by integrating over the region, Ω :

$$59 \quad T_M(t) = \int_{\Omega} M dA, \quad T_C(t) = \int_{\Omega} C dA \quad (1.2)$$

60 These values can be seen in Figure 1.3 (bd) for $T_M(t)$ and (c) for $T_C(t)$.

61 1.1.2 CO_2 Production

62 Since *C. Thermocellum* produces CO_2 as the substrate is consumed, we can track the production of
 63 CO_2 . Following the idea from Dumitrache (2014), we can equate the change in production of CO_2
 64 as time changes by the following equation:

$$65 \quad p_t = \rho G(C)M. \quad (1.3)$$

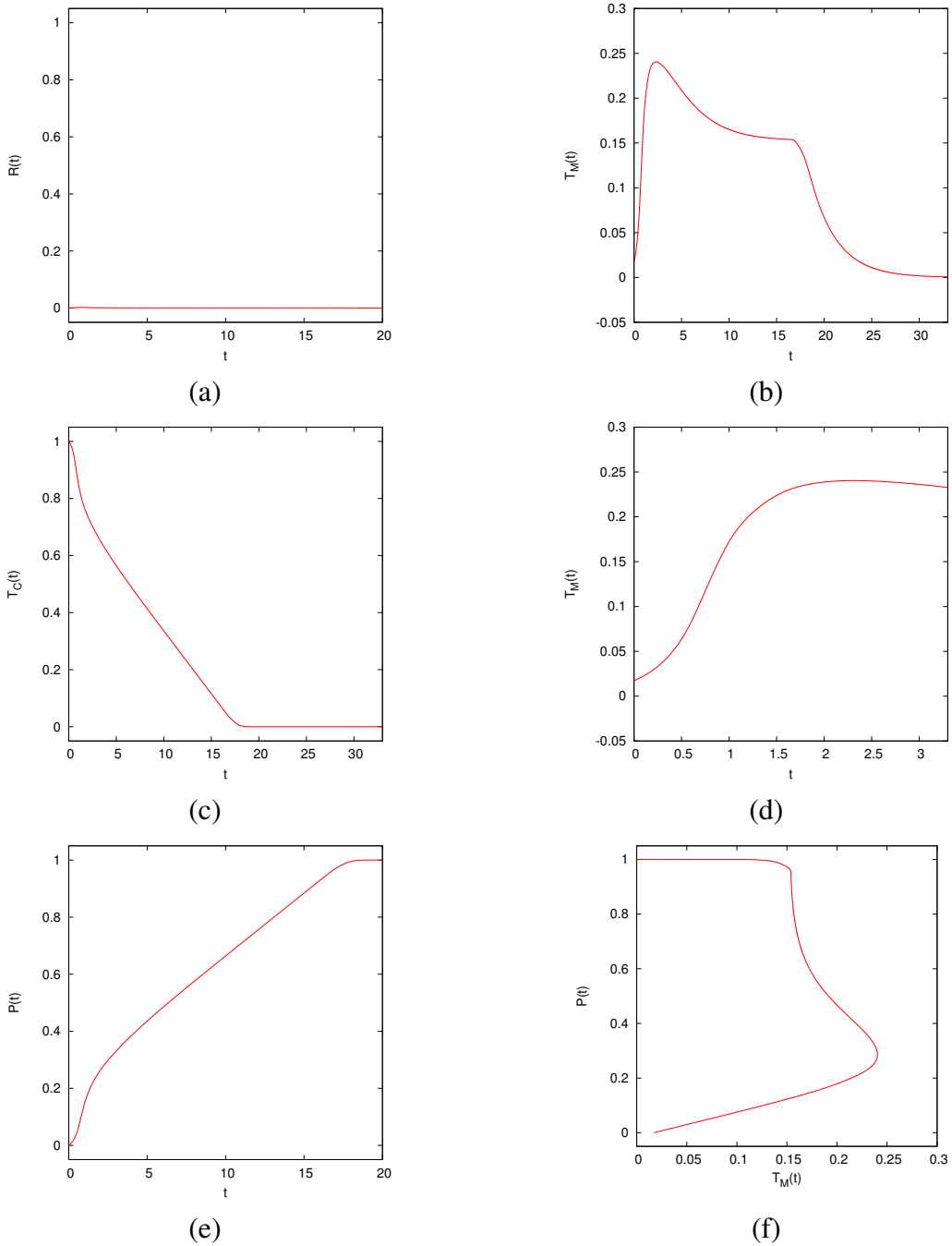


Figure 1.3: Total value of certain qualities from the typical simulation. Here we have: (a) $\mathcal{R}(t)$, the rate of CO_2 production, (b) total M as a function of time, (c) total C as a function of time, (d) total M as a function of time zoomed in from $t = 0$ to $t = 3$, (e) $\mathcal{P}(t)$, the total CO_2 produced, (f) $\mathcal{P}(t)$ as a function of total M . All the graphs are from the same simulation with initial condition of 40 random spherical inoculation points along the $y = 0$ side of the region and another 40 on $y = 1$. A grid of 257×257 was used for this graph. Default parameter set (Appendix A) was used except for $\delta = 10^{-8}$.

⁶⁶ To get the amount of CO_2 produced at a specific time we get,

$$\mathcal{R}(t) = \int_{\Omega} p_t dA = \int_{\Omega} \rho G(C) M dA. \quad (1.4)$$

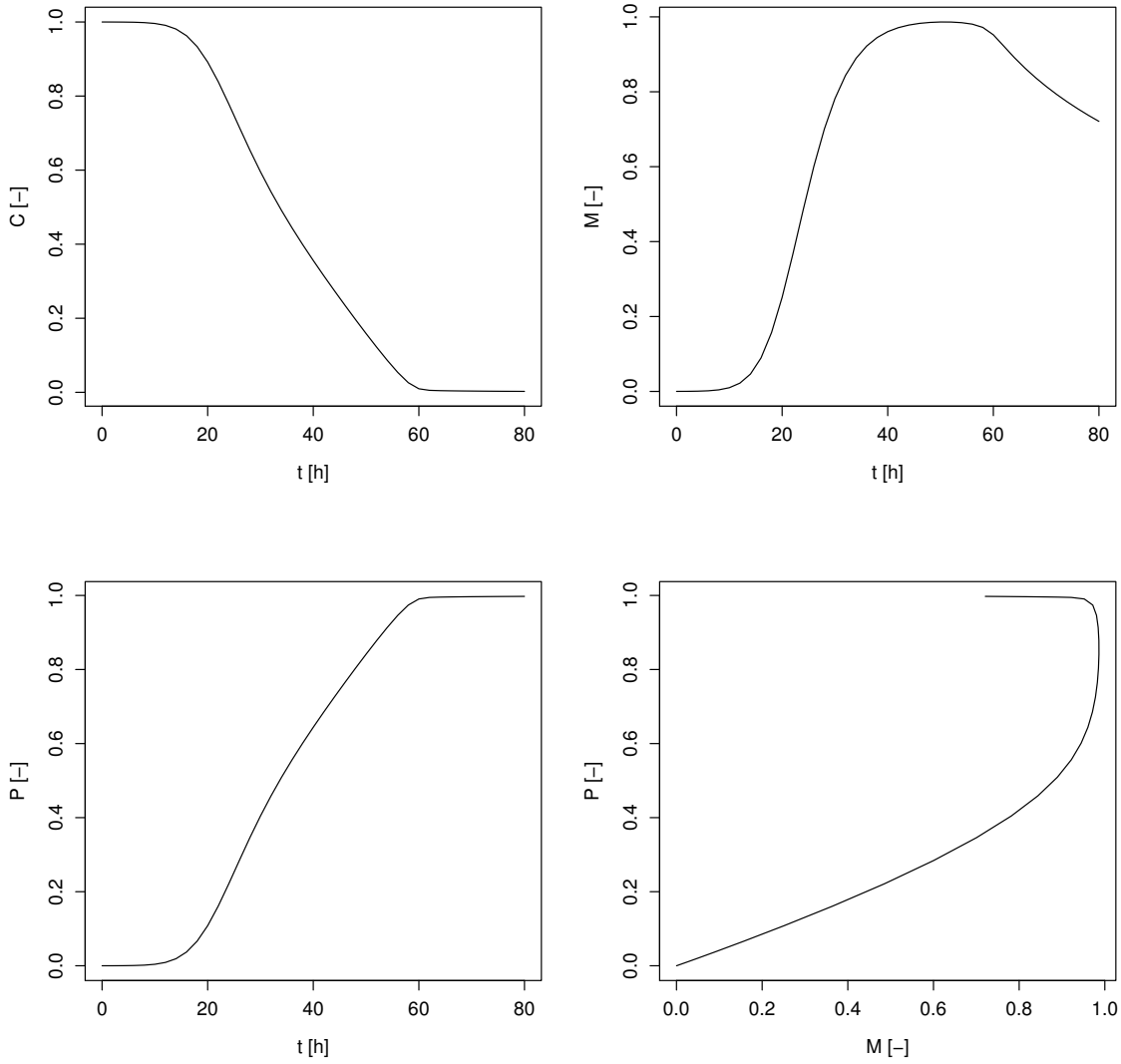


Figure 1.4: A typical model simulation from the simple ODE model. Shown are substrate concentration C (top left, normalised), effective sessile biomass M (top right, relative to the ideal carrying capacity M_∞), and CO_2 product P (bottom left, in moles) as functions of time t . Also shown is the product P vs sessile biomass M (bottom right, in moles).

68 From this we can get the more useful value, the total CO_2 produced until this point.

69

$$\mathcal{P}(t) = \int_0^t \mathcal{R}(s)ds. \quad (1.5)$$

70 The CO_2 amount is calculated by letting $\rho = 1$ and using the numerically computed values for $G(C)M$
71 as a measure. For the same simulation as Figure 1.1, the CO_2 information can be seen in Figure 1.3

72 (a e).

73 The results from Figure 1.3 (c d e f) seems to match the results from the simpler ODE model proposed
74 in Dumitache (2014). Their results can be seen in Figure 1.4. There are a few differences between
75 the two sets of results. In our set of results the global biomass does not approach 1. Our simulations
76 run much longer, in the sense that the parameters were selected to elongate the stationary phase of the
77 bacterial growth since we attempt to encourage the travelling wave solution. This means that certain
78 regions of the graphs become distorted in comparison to Figure 1.4. These differences do not actually
79 change the characteristics of the figures which instead helps validate both sets of results.

80 **1.2 Travelling Wave Analysis**

81 **1.2.1 Spatial Simplification**

82 To simplify the travelling wave analysis we reduce the spatial dimensions to that of a 1D problem.
83 This can be done if initial conditions that are homogenous with respect to y are chosen. The purpose
84 of this spatial simplification is that this will speed up the computations considerable. It will also make
85 visualizations easier to see as certain figures would become too chaotic in 2D. What is done here is
86 more of a psuedo-reduction of dimensions. By reducing the grids from an $n \times m$ grid to an $n \times 4$ grid
87 we have changed the way the problem size scales with finer grids. The problem is still 2D, just now
88 one dimension has been reduced to only 4 grid points of accuracy instead of m points. This does not
89 effect the final result since we only apply this change to problems with appropriate initial conditions.
90 These initial conditions are homogenous in the y direction and thus we do not have any fluctuation
91 between y values for a given x value.

92 One main benefit of changing the grid from $n \times m$ to $n \times 4$ is that the growth of the problem with
93 respect to the fineness of the grid is reduced dramatically. This changes the problem from a $O(n^2)$
94 problem to a $O(n)$. Using the travelling wave 1D initial conditions one simulation is computed with
95 a 513×513 grid, seen at Figure 1.5, and another with a 513×4 grid, seen at Figure 1.7.

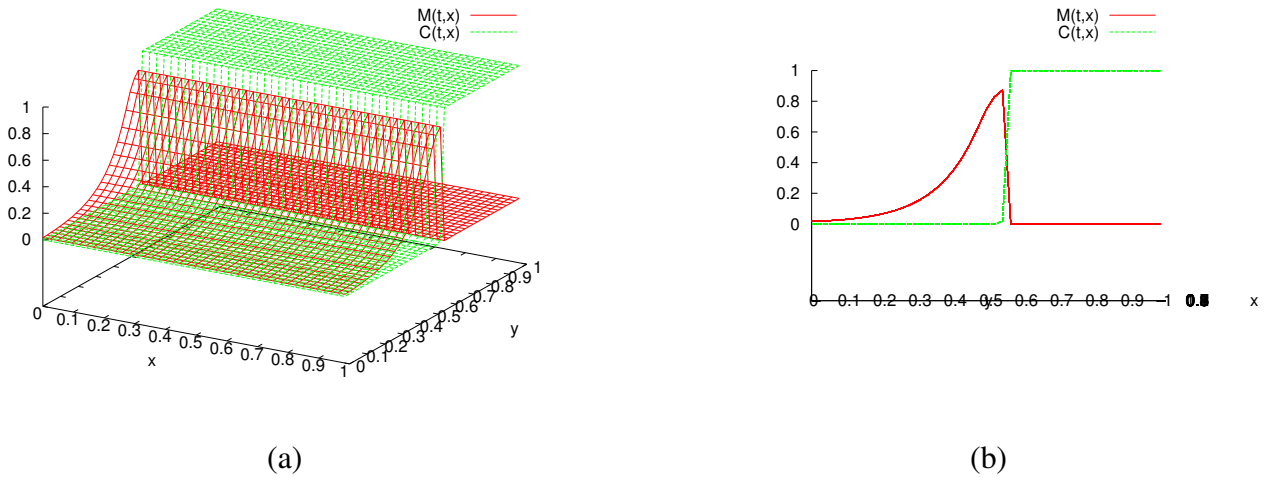


Figure 1.5: Graph of (a) 3D view of $M(t, x, y)$ and $C(t, x, y)$, (b) Side profile view of $M(t, x, y)$ and $C(t, x, y)$ at $t = 40$.

96 Before any changes to the grid can be made, it must be confirmed that there is sufficiently small
 97 fluctuations along the y-axis. To this end, the standard deviation is used as a measure. The standard
 98 deviation is calculated along the y axis for each x value. This gives a numerical quantity for the
 99 measure of dispersal each y value has with another. Here, we use the sample standard deviation for
 100 the sole reason that this single simulation does not represent its own population. Initially, at $t = 0$ the
 101 standard deviation is 0 everywhere (DATA NOT SHOWN). At $t = 40$, Figure 1.6 show the standard
 102 of each y value. After many timesteps have passed the amount of spread is always less then 10^{-14} ,
 103 which is an acceptable degree of consistency. Note that the main inconsistency is at the wave front,
 104 around $x = 5.75$, which is mainly because of the sharp change in values.

105 When simulations are computed with a $n \times 4$ grid, they are still 2D problems. With regards to
 106 visualizations, side profiles could be used on these solutions to present psuedo-1D visualization but
 107 this is not ideal. To visualize the solutions in true 1D the we use \bar{M} and \bar{C} as averaged values of the
 108 solutions along the y-axis. This is computed after the solution has been determined and is independent
 109 of the actual compuations for M and C. So by taking the average of the points along the y-axis we
 110 can get a 2D plot as seen in Figure 1.7.

111 This means that the system can be reduced to a 1D problem. With initial conditions that are homoge-
 112 nous with respect to y, we can greatly reduce the accuracy in the one axis. Once the y-axis reduced,

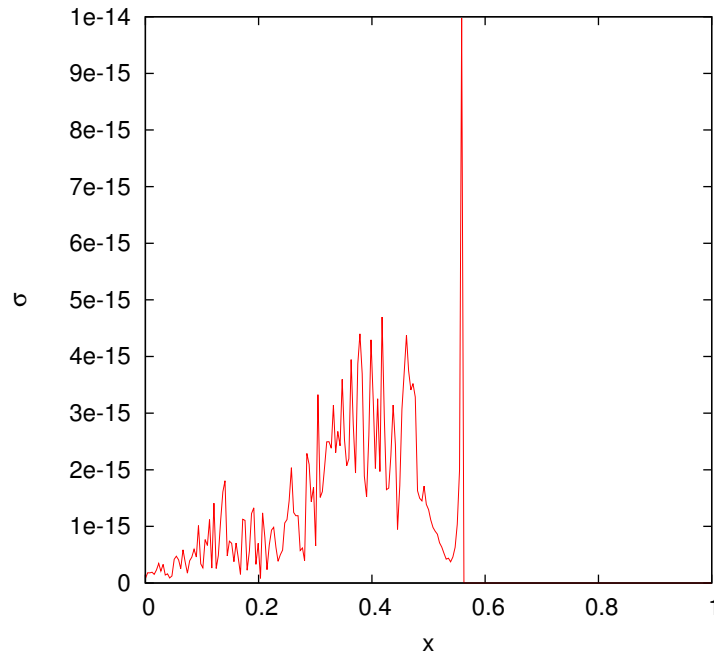


Figure 1.6: The standard deviation at the same time as the above graphs

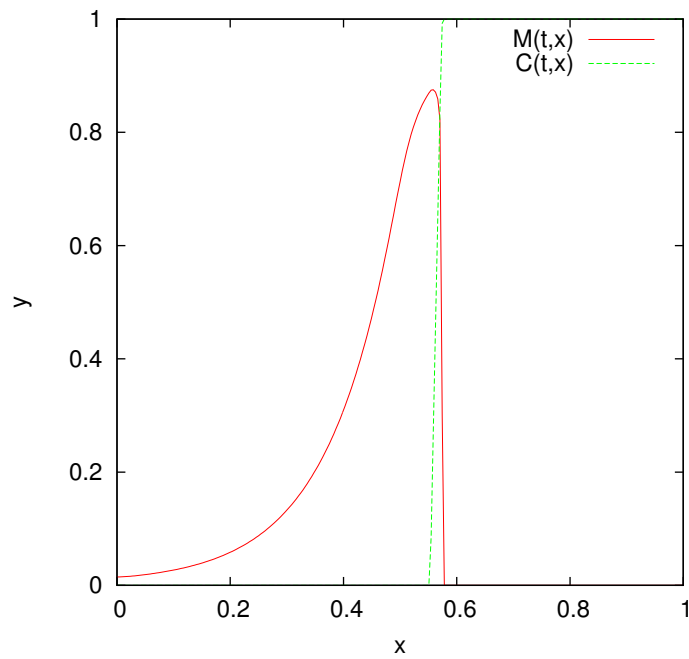


Figure 1.7: Graph of $M(2,y)$ and $C(2,y)$, now reduced to a 2D plot.

¹¹³ we can also ignore it for visualizations, only using the x-z axis and plotting the values of \bar{M} and \bar{C} .

¹¹⁴ **1.2.2 Travelling Wave Solution**

¹¹⁵ Looking at Figure 1.7 more closely it seems, from the given shape, we have a travelling wave solution.

¹¹⁶ This sense is strengthed by showing the time evolution, as seen in Figure 1.8. It is clear here that the
¹¹⁷ shape of the solution is consistent enough to suggest the existence of a travelling wave solution.

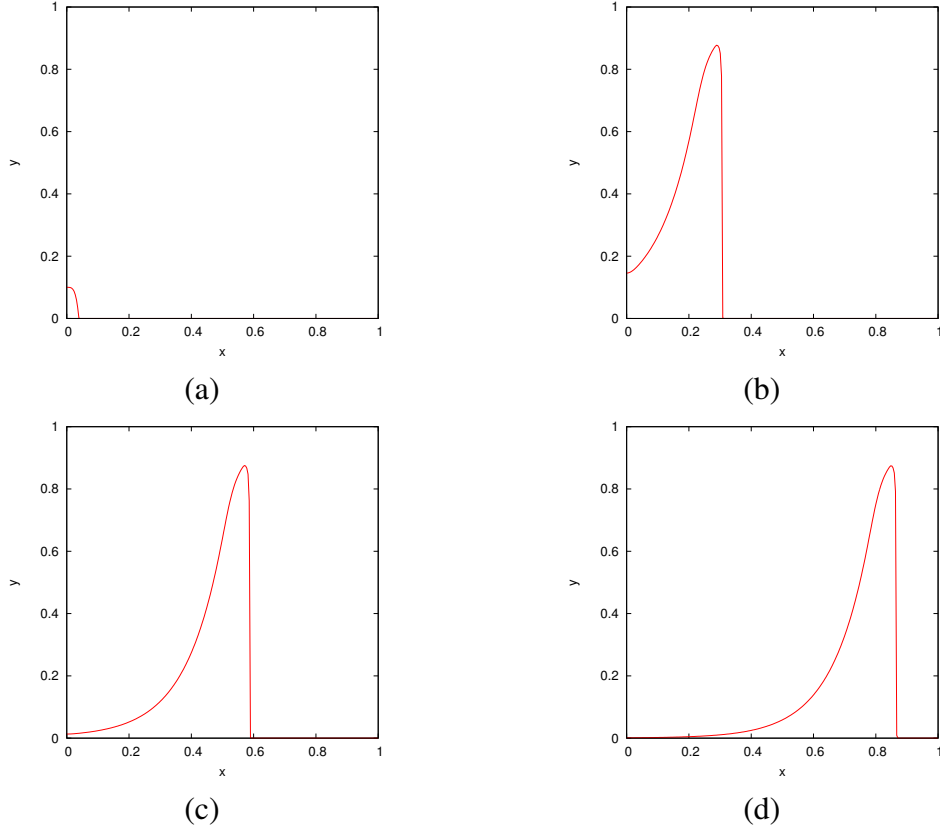


Figure 1.8: Solutions of $M(x, t)$ and $C(x, t)$ at (a) $t = 0$, (b) $t = 20$, (c) $= 40$, (d) $= 60$. This was run on a 513×4 grid.

¹¹⁸ Around $t = 60$, when the travelling wave solution appears to have fully formed. This can be confirmed
¹¹⁹ if we can show that we can write the solution $M(x, t)$ as $M(x + ct)$, where c is the wavespeed of
¹²⁰ the solution. Visually, multiple timesteps horizontally translated onto each other would show this. If
¹²¹ the horizontal translations are all multiples of the same number then we have shown that a constant
¹²² speed exists. If the shape of all the timesteps match then a constant shape then strong evidence that
¹²³ a constant shape exists would be shown. We can numerically approximate the value for c by looking
¹²⁴ at how fast the peak of the wave travels. The location of the wave peak is the x coordinate that

125 corresponds to the largest M value. Recall that we are dealing with a psuedo-1D problem, so there
 126 does not need to be any consideration for an (x, y) coordinate. For this case, we used the GNUPLOT
 127 software to fit a linear model, $f(x) = mx + b$, to the last half of the wave peaks path, seen in Figure
 128 1.9. The last half of the values were used instead of the whole set of values because only for the
 129 former do we have a fully formed travelling wave. The value of m in $f(x)$ is the approximation for
 130 the wavespeed, c .

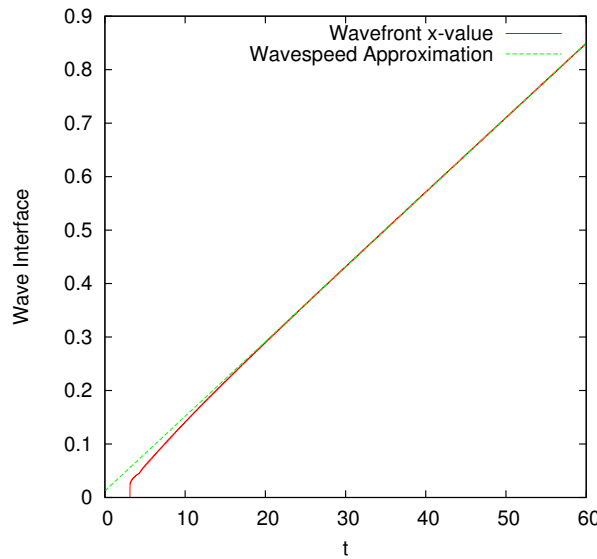


Figure 1.9: The x location of the wave peak as a function of t . The red line is the wave peak location extracted from the simulation results. The green line is the function $f(x) = cx + b$ with c as the wavespeed, found by fitting the model to the second half of x values. The simulation results used here are from the solution shown in the previous Figure.

131 With an approximation for c , the solutions of Figure 1.8 can be represented as $M(x + c(t_0 - t_n))$,
 132 where t_0 is a reference point for the other timesteps, not the time value $t = 0$. The values of t_n are
 133 the times for the other solutions, each can be horizontally translated on top of each other by changing
 134 the time value so that they all are equivalent to t_0 . This works because we assume *a priori* that the we
 135 are handelling travelling wave solutions. With that we can just change the t value in $M(x + ct)$ to get
 136 the multiple timesteps at the same point. In Figure 1.10 multiple timesteps of Figure 1.8 are shown
 137 on top of each other. The shape of each timestep is very similar throughout, only differing slightly at
 138 the tail.

139 Based on the above evidence, we can say that a travelling wave solution has been shown to exist for a

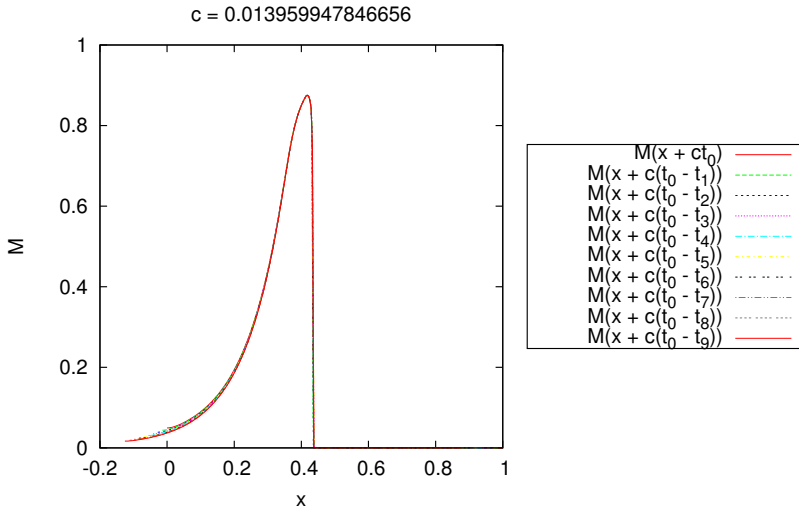


Figure 1.10: Solutions of M that are represented as $M(x + ct)$ *a priori*. The multiple timesteps are translated on top of another by changing

140 single initial condition and particular set of parameters. This leads to two logical extensions, looking
 141 at the stability of the travelling wave solution based on initial condition and investigating the effect
 142 the parameters have on the travelling wave solution.

143 1.2.3 Travelling Wave Stability

144 Based on the previous example, there seems to exist a travelling wave solution. The next step is
 145 looking at how different initial conditions could still result in a travelling wave solution. For this
 146 we specifically look at the stability of the solution, does it attract nearby solution into becoming a
 147 travelling wave solution or is it only for specific cases that one results. This will help confirm that the
 148 existence of the travelling wave solution is not depended on the single choice of initial condition.

149 To test this we take an initial condition that is not inherently one dimensional and see if it approaches
 150 to the one dimension property. The choice of IC is to have multiple random spherical inoculation
 151 points along the $y = 0$ side of the region. Specifically, we use (x_r, y_r) to represent the center of each
 152 random inoculation point. Here $x_r \in \mathcal{R}$ and $y_r \in [0, 0.1]$.

153 The equation used for each random spherical inoculation point is,

154

$$M = \frac{-h}{d^2} ((x - x_r)^2 + (y - y_r)^2) + h, \quad M \geq 0. \quad (1.6)$$

155 Random inoculation points add to each other if they overlap. After all the inoculation points have
 156 been generated, every value is divide by the total amount of biomass. This lets the initial condition
 157 become a representation for the distribution of random inoculation points in terms of the total amount
 158 generated. A time evolution of the simulation with the above initial condition can been seen in Figure
 159 1.11. Here it can be observed that the solution M appears to slowly converge to a 1D problem. This
 160 cannot be fully seen since the wave propagation reaches the end of the region before it can become
 161 fully one dimensional.

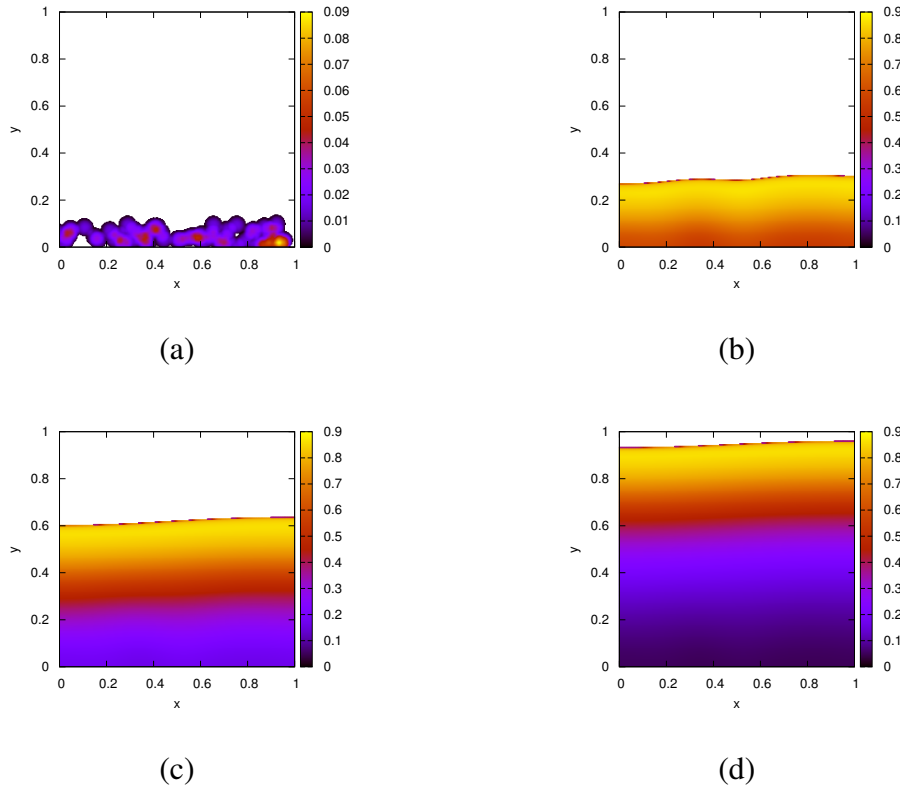


Figure 1.11: Plots of the simulation with random spherical inoculation points centered in the region $(x, y) \in [0, 0] \times [1, 0.1]$. The solutions are shown at (a) $t = 0$, (b) $t = 10$, (c) $t = 20$, and (d) $t = 30$. Each solution is computed on a 513×513 grid.

162 We can quantitatively see the behaviour of this convergence by calculating the measure of spread at

163 the wave front. This can be achieved by calculating the standard deviation of y coordinate for each
 164 x coordinate. By tracking the largest y value with a non-zero M for each x value we can generate a
 165 sample data set of the wavefront. The wavefront is used instead of other points of interest, such as
 166 the wave peak, because it is the most consistent of characteristics that can be easily tracked. As seen
 167 in Figure 1.6, the wave peak had the largest spread among all other values.

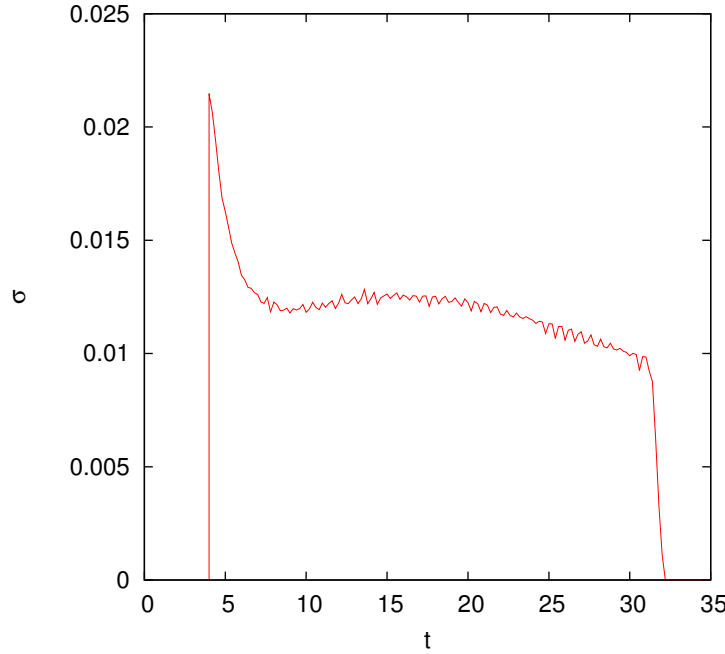


Figure 1.12: The standard deviation of the wavefront interface as a function of time. The wavefront references the largest y coordinate with $M > 0.001$ for each x coordinate. The choice of using $M > 0.001$ is because we want to ignore the small values (10^{-100}) that arise from the diffusion right at the wave front. This simulation is the same as the previous Figure.

168 Taking the sample standard deviation of this set results in the measure of spread for the wavefront. The
 169 sample standard deviation was used since this one example does not represent the whole population
 170 of solutions. The idea is that, for a solution that converges to one-dimensionality, the y location of
 171 the wavefront should be converging to similar values. This means that the standard deviation would
 172 converge to zero. The standard deviation of the wavefront as a function of time of the simulation
 173 ran in Figure 1.11 can be seen in Figure 1.12. Here is shows that the solution is converging to zero,
 174 however not monotonically.

175 For the numerical computation of the wavefront, the largest y values greater than 0.001 was used

176 instead of 0. The reason is that there are very small values of around 10e-200 that arise due to the
 177 diffusion that were not adequate representations of the wavefront.

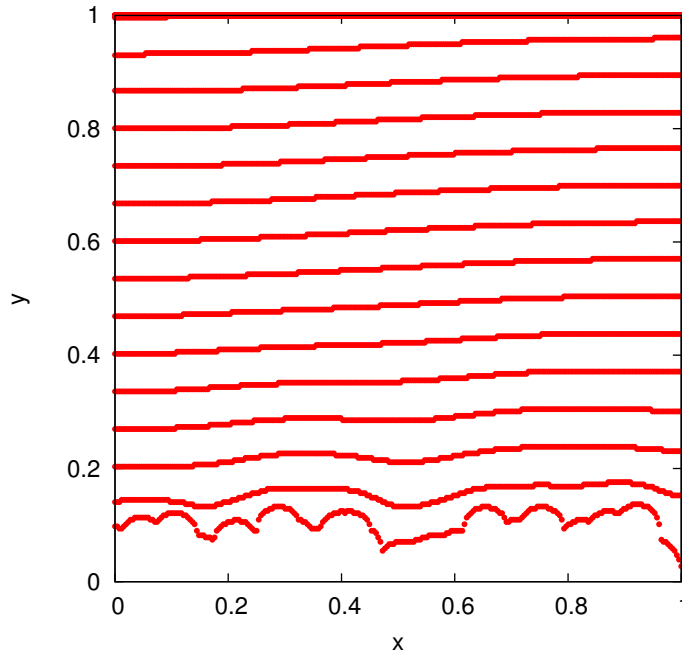


Figure 1.13: The wavefront shape of multiple timesteps. Each wavefront has a difference in time by 2, i.e. they are at $t = 4, 6, 8, \dots, 58, 60$. The simulation results are the same as the previous Figures, using the default parameter values with a grid size 513×513 .

178 Another interesting item to investigate is the actual shape of the wavefront. Figure 1.13 shows only
 179 the wavefront shape for multiple timesteps. The wavefront shape is the same dataset of points used to
 180 calculate the standard deviation of the wavefront interface. Of interest is that the wavefront appears
 181 to move at a constant speed, since each wavefront shown is equidistant from the next.

182 1.2.4 Parameter Effect on Wavespeed

183 The idea here is to confirm that the travelling wave solution seen before are not for the one specific
 184 parameter set. From this we can also see how the wavespeed of the travelling wave solution changes
 185 as a function of the different model parameters.

186 For this an automated script was created that checks, for each timestep, if M is travelling wave solu-
 187 tion based on the solution of M from a number of timesteps previous. From this check, a wavespeed
 188 needs to be approximated based on the distance between the two solutions. If this approximated

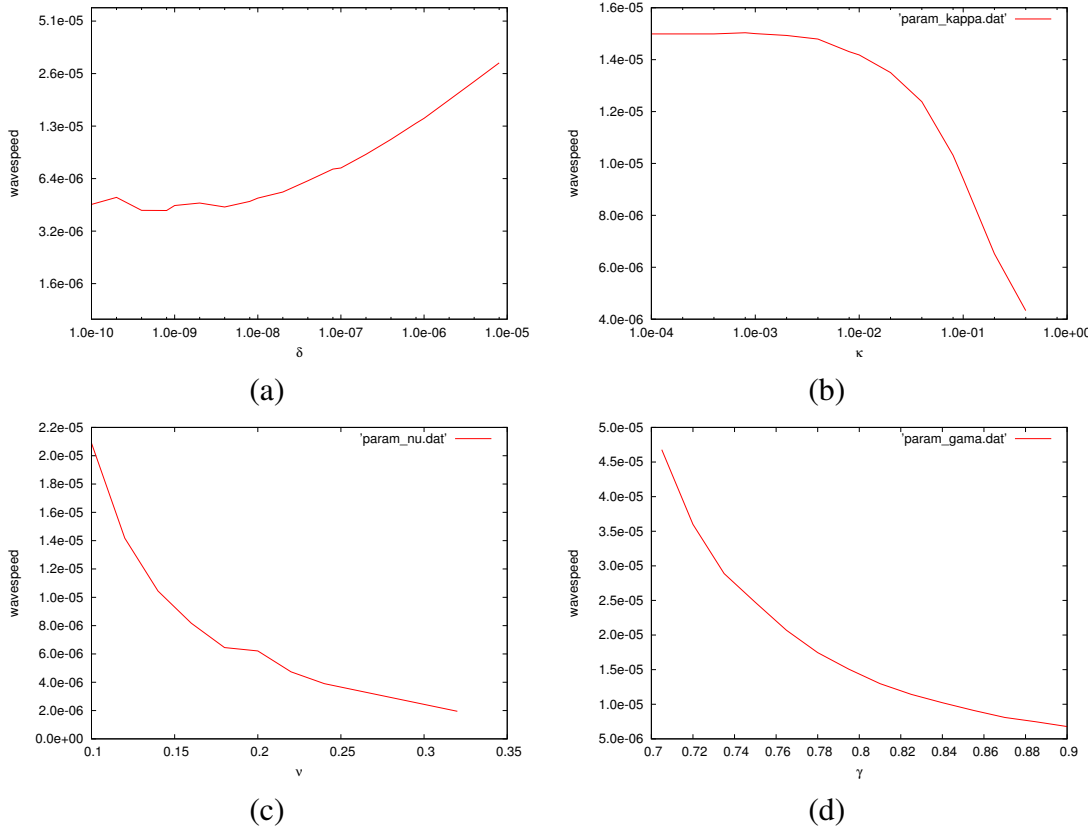


Figure 1.14: The value of c as parameter (a) δ , (b) κ , (c) ν , and (d) γ are changed. Note that (a) and (b) have logscales due to the selection of parameter values. Each of these were calculated with the same setup as the travelling solution previously done. The grid size for each was 513×4 and a time step of $\Delta t = 0.001$ was used.

189 wavespeed is matched throughout all the x values, then a travelling wave solution is assumed to exist
 190 at that timestep. With this script, we can try the same simulation as Figure 1.8 with different parameter
 191 values.

192 For each parameter, δ , κ , ν , γ , the range of values chosen were so relatively arbitrary. Figure 1.14
 193 shows the results of the wavespeed for each parameter changes. Mainly it was so that the solution
 194 did not propagate too fast and hit the end of the region before developing into a full travelling wave
 195 solution. Generally when the travelling wave does not form it is because the wave front propagates
 196 to the end of the region faster than the tail of the travelling wave can decrease to 0. In the case of ν ,
 197 any larger values than the selected range resulted in biomass that died faster than it could grow, and
 198 thus no travelling wave solution exists. There did not appear to be any cases where a travelling wave
 199 solution could not form.

200 Since, for each of the choosen parameters, a travelling wave solution was seen to exist, it can be said
 201 that the choice of parameter in Figure 1.8 was not the only reason for the travellin wave solutions
 202 existance.

203 **1.3 Spatial Effects**

204 There are many spatial effect that can exist here because of the diffusion term in the biomass. We
 205 now try observing any differences in the behaviour of the system based on spatially different initial
 206 conditions. This will show if there is any noticeable differences in the behaviour of the system based
 207 solely on the placement of initial biomass. There will be two methods to compare the different
 208 simulations: visually and by monitoring the amount of CO_2 produced. The visual inspection is a
 209 logical comparison to use, the CO_2 is choosen since it essentially provides a measure of the activity
 210 in the system. The CO_2 is also used in the experiments conducted in Dumitrache (2014).

211 To measure the difference, two simulations will be run with varying initial conditions. One simulation
 212 will have the initial condition evenly spread along one side of the region. The other will have all
 213 the initial condition clumped in single corner. This will replicate the two possible extremes for the
 214 location of biomass.

215 Since the only difference is the initial conditions, and since an equal start must be assured, the selec-
 216 tion of initial condition is important. The equally dispersed initial condition needs to have as much
 217 surface area exposed as reasonably possible. To this end, multiple spherical innoculation points,
 218 equidistance from each other, are used along the $y = 0$ side of Ω . Here we use (x_e, y_e) as the center
 219 of the evenly distributed innoculation points. The value of (x_e, y_e) depends on the number of points
 220 choosen for the simulation.

221

$$M = \frac{-h}{d^2}((x - x_e)^2 + (y - y_e)^2) + h \quad (1.7)$$

222 For the clumped initial condition, we choose another spherical innoculation point so that it is similar

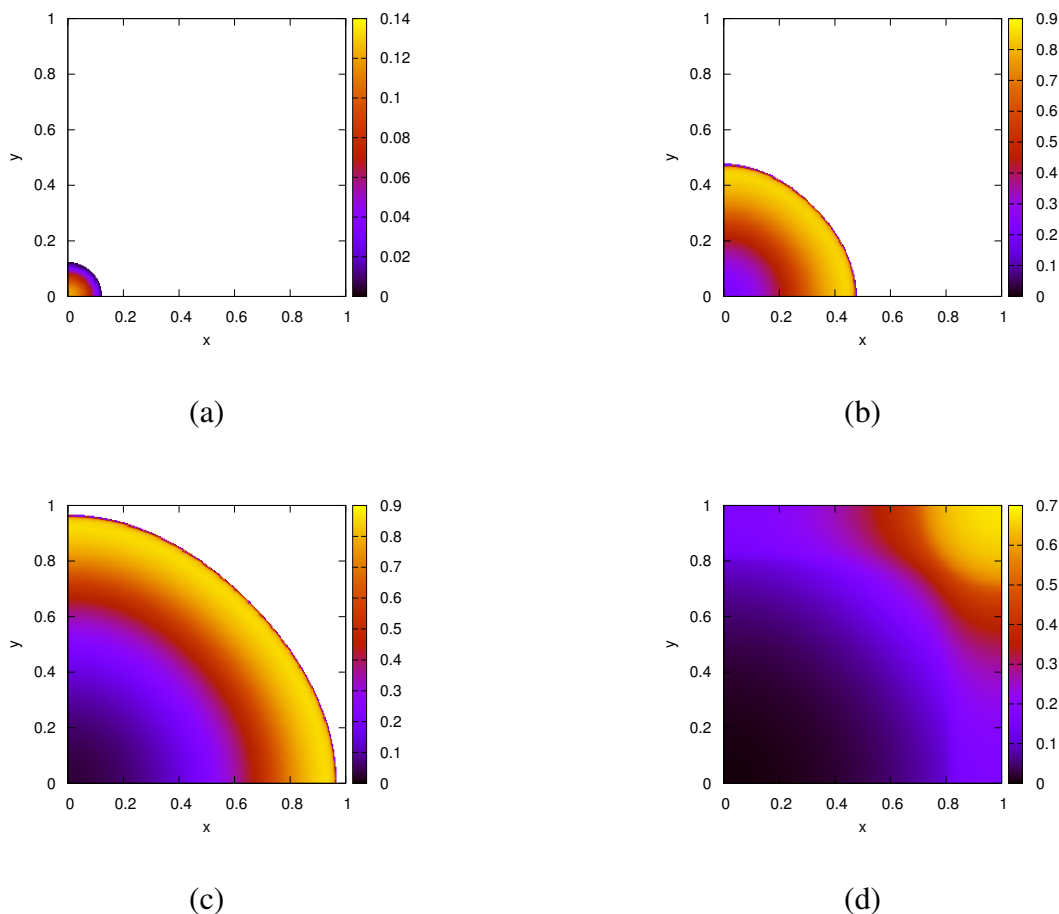


Figure 1.15: This shows the time evolution for the clumped initial condition at (a) $t = 0$, (b) $t = 16$, (c) $t = 32$, (d) $t = 48$. Here default parameters are used on a grid size of 513×513 .

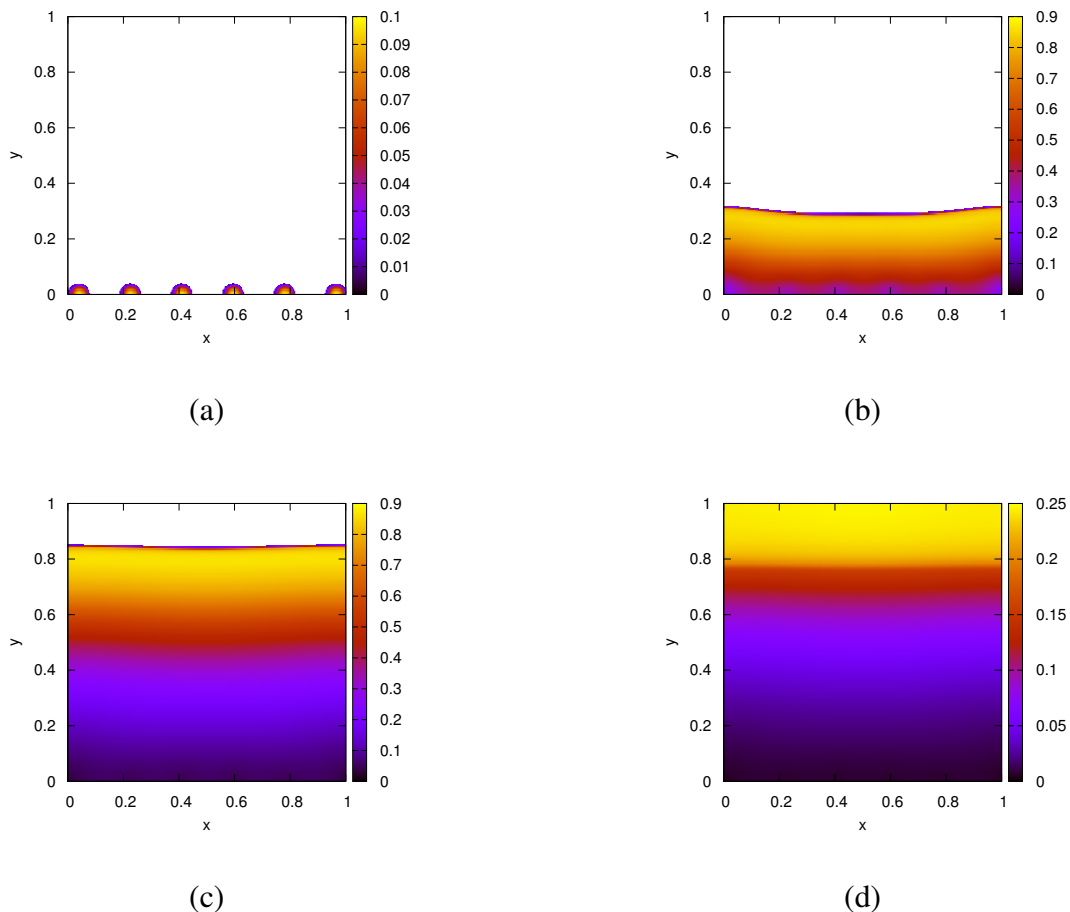


Figure 1.16: This shows the time evolution for the evenly distributed initial condition at (a) $t = 0$, (b) $t = 16$, (c) $t = 32$, (d) $t = 48$. Here default parameters are used on a grid size of 513×513 .

223 to the evenly distributed initial condition. Here, we need only a single inoculation point, centered at
 224 the corner $(0, 0)$. The choice of inoculation center is so that the initial biomass is as concentrated as
 225 possible, while still retaining a spherical shape. The initial condition for the clumped biomass is as
 226 follows,

$$227 \quad M = \frac{-1}{(2hd^2 \cdot num)^{\frac{1}{3}}} (x^2 + y^2) + (2hd^2 \cdot num)^{\frac{1}{3}}. \quad (1.8)$$

228 Here the coefficents have been choosen so that the two initial conditions have the same amount of
 229 biomass. The value of num is to represent the number of inoculation points in the evenly distributed
 230 initial condition.

231 Figure 1.15-1.16 shows the time evolution of both initial conditions. Here we arbitrarily select $num =$
 232 6.

233 It becomes easier to see the difference between the two spatially difference problems when CO_2
 234 production is taken into account. In Figure 1.17 it is clear that there is a substantial difference between
 235 the CO_2 production of both cases. However, this difference does not show an inconsitency with
 236 spatially different initial conditions. Closer observation reveals that the two simulations have similar
 237 qualitative behaviours, which is the important information to take from this.

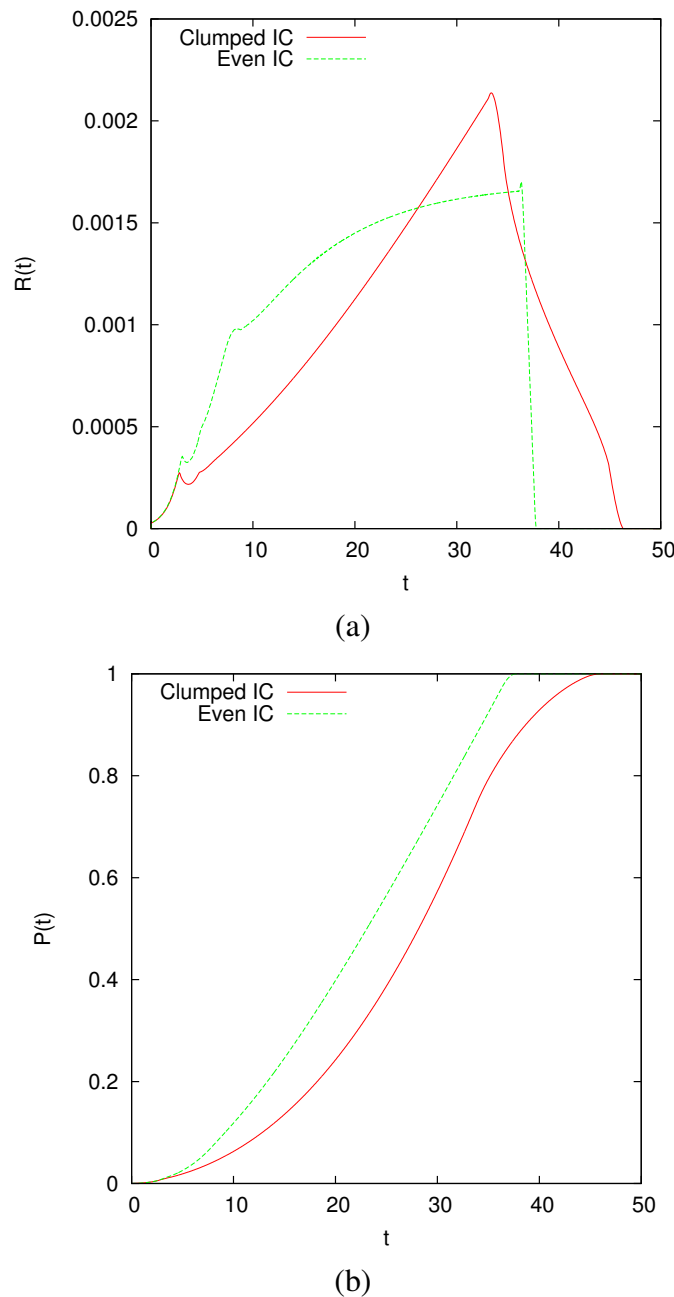


Figure 1.17: A plot of (a) $\mathcal{R}(t)$ and (b) $\mathcal{P}(t)$. These are extracted from the same simulation done in the two previous figures.

²³⁸ References

- ²³⁹ R. Barrett, M. Berry, Chan T.F., J. Demmel, J. Donato, J. Dongarra, V. Eijkhout, R. Pozo, C. Romine, and H. van der Vorst. *Templates for the Solution of Linear Systems: Building Blocks for Iterative Methods*. Society for Industrial and Applied Mathematics, 1st edition, 1987.
- ²⁴² J.C. Butcher. *Numerical Methods for Ordinary Differential Equations*. Wiley, 2nd edition, June 2008.
- ²⁴³ A Dumitrache. *Understanding Biofilms of Anaerobic, Thermophilic and Cellulolytic Bacteria: A Study towards the Advancement of Consolidated Bioprocessing Strategies*. PhD thesis, University of Toronto, 2014.
- ²⁴⁶ HJ Eberl and L Demaret. A finite difference scheme for a doubly degenerate diffusionreaction equation arising in microbial ecology. *Electron. J. Differential Equations*, page 7795, 2007.
- ²⁴⁸ HJ Eberl, DF Parker, and MCM van Loosdrecht. A new deterministic spatio-temporal continuum model for biofilm development. *Journal of Theoretical Medicine*, pages 161–175, 2001.
- ²⁵⁰ S. Geršgorin. über die abgrenzung der eigenwerte einer matrix. *Bulletin de l'Académie des Sciences de l'URSS. Classe des sciences mathématiques et na*, pages 749–754, 1931.
- ²⁵² DR Noguera, G Pizarro, DA Stahl, and BE Rittmann. Simulation of multispecies biofilm development in three dimensions. *Water Science and Technology*, 39:123–130, 1999.
- ²⁵⁴ BE Rittmann and PL McCarty. Model of steady-state biofilm kinetics. *Biotechnology and Bioengineering*, 22:2343–2357, 1980.
- ²⁵⁶ Y. Saad. *Iterative Methods for Sparse Linear Systems*. Society for Industrial and Applied Mathematic, 2nd edition, 2003.

258 S Sirca and M Horvat. *Computational Methods for Physicistsl: Compendium for Students*. Springer,
259 2012.

260 Z-W Wang, S-H Lee, JG Elkins, and JL Morrell-Falvey. Spatial and temporal dynamics of cellulose
261 degradation and biofilm formation by caldicellulosiruptor obsidiansis and clostridium thermocel-
262 lum. *AMB Express*, 1:30, 2011.

263 **Appendix A**

264 **Default Parameter Values**

265 The default parameter values used for simulation are listed in the follow table. Unless stated, every
266 simulation uses these values.

Parameter	Symbol	Value
-	α	4
-	β	4
Death rate	ν	0.12
Half-concentration rate	κ	10^{-3}
Yield rate	γ	0.80
Diffusion constant	δ	10^{-4}
Initial condition height	h	0.1
Initial condition depth	d	$\frac{5}{127}$
Number of grid points	nm	513×513
Grid size	Δx	$\frac{1}{513}$
Time step	Δt	10^{-3}

Table A.1: The listing of default parameter values used for most simulations.